JOURNAL OF GEOPHYSICAL RESEARCH, VOL. 85, NO. A5, PAGES 2124-2130, MAY 1, 1980

A Macroscopic Profile of the Typical Quasi-Perpendicular Bow Shock: Isee 1 and 2

E. W. GREENSTADT,[1] C. T. RUSSELL,[2] J. T. GOSLING,[3] S. J. BAME,[3] G. PASCHMANN,[4] G. K. PARKS,[5] K. A. ANDERSON,[6] F. L. SCARF,[1] R. R. ANDERSON,[7] D. A. GURNETT,[7] R. P. LIN,[6] C. S. LIN,[5] AND H. RÈME[8]

Field and particle properties of the bow shock recorded on November 5, 1977, identified earlier as stable features by comparison of Isee 1 and 2 data, are examined macroscopically. The extent to which the shock was in a 'typical' state is described, and multidiagnostic observations are combined to define the shock profile, which, in this known case, is reminiscent of composite portraits assembled from earlier studies. A foot, a principal wave front gradient, and a postfront overshoot characterized the magnetic field. Various particle measurements revealed corresponding structural elements, including a bimodal ion energy distribution whose two peaks were at roughly the solar wind streaming energy and 2 to 3 times the streaming energy. The electrons were thermalized before the principal sharp magnetic gradient; the ions were partially randomized at the gradient, but the ion thermalization process was not completed until long after the gradient was crossed. The second peak of the ion distribution represented a separate group of reflected particles upstream of the main magnetic gradient that retained its identity for an appreciable distance behind the front before being merged by thermalization into the general distribution. This separate group included a northward proton flux in front of, but not immediately behind, the front. The group ultimately became thermalized through a series of very regular oscillations. The decrease in solar wind bulk velocity at the front exceeded the sum of that calculated from an idealized first-order model of the rise in potential opposing the flow, plus the proton heating, leaving proton reflection and wave radiation and dispersion as candidates to account for the discrepancy. Plasma wave activity, at ion acoustic frequencies, was most intense in the foot and at the front and appeared to be enhanced at the outer boundary of the reflected particles.

INTRODUCTION

One phenomenon of great interest in space plasma physics is the collisionless shock wave, best represented by the bow shock of the earth, and the first such opportunity to observe the shock with two closely spaced satellites is afforded by the Isee 1/Isee 2 satellite pair. A number of papers covering the initial observations, as recorded for the most part by individual detectors, were presented at the thirteenth ESLAB Symposium held in Innsbruck, Austria, in June of 1978 and were collected for publication as a group in *Space Science Reviews* [*Knott et al.*, 1979]. Additional papers covering special topics have also been published [*Bame et al.*, 1978; *Gosling et al.*, 1978]. In this report we offer the first attempt to gather and collate the data from a group of instruments measuring their respective profiles of the bow shock all at once.

This first study exploits the best available case, that of a 'typical,' somewhat complicated shock configuration. The report that follows covers the general qualitative aspects of the chosen shock from a predominantly macroscopic point of view. That is, the objective here is to expose the overall structure of the shock on a macroscopic scale; in this treatment, departures from equilibrium will be noted but not pursued in further detail. The chosen case was typical according to criteria dealing with the upstream plasma conditions, the location of the shock, and the location of the spacecraft observations.

There are two beneficial results of using paired observations to separate space and time effects in dynamic plasma phenomena. First, the thicknesses and scale factors of various features can be estimated from their measured velocities in the spacecraft frame, yielding a quantitative portrayal of the phenomenon under study and hence a basis for valid comparisons with theory. Second, the stability, or reproducibility, of plasma structures can be verified or discounted and study effort directed accordingly. The general similarity of the profiles of the November 5 shock crossings by Isee 1 and Isee 2 was shown in earlier papers [*Russell and Greenstadt*, 1979;.*Bame et al.*, 1979], so in the present report we display the data almost entirely from Isee 1 with knowledge that the features to which we call attention characterized the shock for at least several minutes. Preliminary numerical dimensions of some elements of the November 5 shock were given by *Russell and Greenstadt* [1979] and *Bame et al.* [1979].

The reader interested in the prevailing status of satellite-based experimental investigation of plasma shocks may be interested in three recent reviews written with the intention of documenting the current position and future direction of shock study at the onset of the Isee epoch: *Greenstadt* [1976], *Formisano* [1977], and *Greenstadt and Fredricks* [1979].

[1] Space Sciences Department, TRW Defense and Space Systems Group, Redondo Beach, California 90278.
[2] Institute of Geophysics and Planetary Physics, University of California at Los Angeles, Los Angeles, California 90024.
[3] Los Alamos Scientific Laboratory, University of California, Los Alamos, New Mexico 87544.
[4] Max-Planck-Institut für Physik und Astrophysik, Institut für Extraterrestrische Physik, 8046 Garching, Munich, West Germany.
[5] Geophysics Program, University of Washington, Seattle, Washington 98195.
[6] Space Sciences Laboratory, University of California at Berkeley, Berkeley, California 94720.
[7] Department of Physics and Astronomy, University of Iowa, Iowa City, Iowa 52242.
[8] University of Toulouse, Toulouse, France.

Paper number 80A0063.
0148-0227/80/080A-0063$01.00

MEASUREMENTS

The instruments whose measurements have been collected for this study are listed below, together with brief comments necessary for this report and references where further details can be obtained.

Magnetometer. In this paper we show only the magnitude of the ambient magnetic field taken from vector samples made by the University of California at Los Angeles (UCLA) magnetometer, ±4 mγ every 0.25 s [*Russell,* 1978; *Russell and Greenstadt,* 1979].

Fast plasma analyzer. Ion spectra and proton and electron moments representing fluid parameters were provided by the pair of '2D' quadraspherical electrostatic analyzers and processing techniques of Los Alamos Scientific Laboratories and the Max-Planck-Institute for Extraterrestrial Physics (LASL/MPE). The analyzers measured the plasma components within ±55° of the ecliptic plane, obtaining complete spectral and angular samples every 3 s (i.e., every spin period). At the low data rate of this report, only every fourth spectrum was transmitted, every 12 s. In cold solar wind, only partial or fragmented ion distributions were recorded, so reliable moments could only be derived from spectra in the magnetosheath. Proton parameters are plotted accordingly in this paper with values first appearing in or behind the shock front after radical variations from sample to sample had ceased. Spectral samples reproduced here are count rate distributions that overstate the high-energy side of the curves. Proton moments derived in and just behind the shock front, where distributions were double peaked or highly skewed, are reliable, but 'temperatures' associated with them should be read with caution for such irregular forms [*Bame et al.,* 1979; *Paschmann et al.,* 1978].

Fixed voltage analyzer. The fluxes of electrons and protons moving within a 7.5° cone toward north ecliptic pole (*Z* axis) are displayed for the lowest (1.5 keV) energy step of the energetic particle flux experiment of the University of California at Berkeley (UCB). The fluxes were sampled every 0.25 s [*Anderson et al.,* 1978; *Parks et al.,* 1978].

Plasma wave analyzer. Electric field turbulence was measured by the electric dipole antennas supplied by the University of Iowa (UI). Data in both dynamic spectrogram form and from selected channels of the on-board multichannel filters are used in this report [*Gurnett et al.,* 1978, 1979].

CROSSING CONDITIONS

Shock-Crossing Geometry

The relative positions of Isee 1 and 2, the crossing sequence, and the magnetic shock profiles are illustrated in Figure 1. Isee 1, earthward and ahead of its companion vehicle inbound, crossed the shock at about 1322:30, entering the variable elevated field of the magnetosheath. While Isee 1 penetrated the sheath, the shock moved outward until Isee 2 encountered it 0.5 min later. The projected distance between the satellites along the assumed direction of shock motion, namely, the shock normal, was 228 km, so the exact time delay between the sharpest magnetic gradients, 33 s, suggests that the shock was expanding locally with a velocity of 6.9 km/s in the spacecraft frame. In the earth's frame, with the spacecraft motion subtracted, the shock's outward speed was about 5.5 km/s. The times and field levels marked in Figure 1 will be cited later in this report.

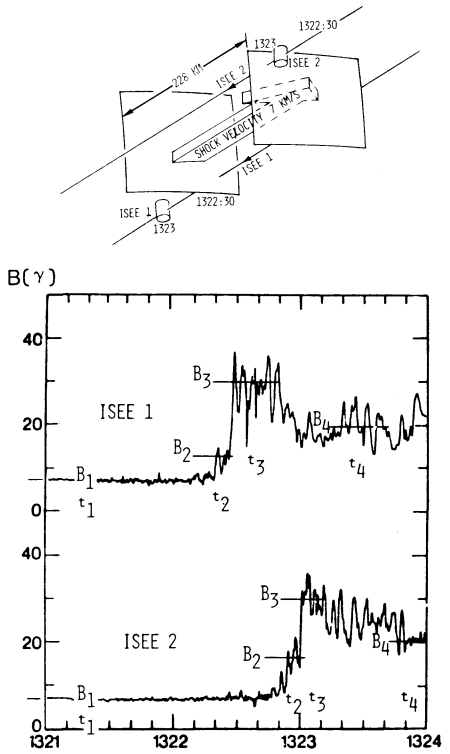

Fig. 1. The shock encounters at 1323. Isee 1 was in the magnetosheath behind the shock, having crossed it at 1322:30, while the shock, having moved outward, was just meeting Isee 2. Marked times and field levels are used in a later calculation in the text.

Shock Structural Parameters

Figure 2 displays the configuration of shock, interplanetary magnetic field (IMF), and spacecraft location at the time of observation, together with a summary of the solar wind parameters in relation to their statistical distributions. The uppermost sketch is a schematic view of the bow shock showing the *X-Y* (ecliptic) plane, the *B-X* plane containing the IMF, and the position of the paired Isee crossings not far from the subsolar point. The coordinates of the spacecraft were $R = (13.18, -5.19, 6.5)\ R_E$; the components of the IMF just before the inbound crossing were $B = (-1.8, 6.6, 1.1)\ \gamma$. The shock was almost exactly at its average location when crossed. Table 1 summarizes the solar wind conditions upstream from the bow shock. The upstream values of V, N, and T_p were obtained from measurements by the crossed-fan instrument of LASL on Isee 1 and checked against those of the Frascati solar wind experiment on Isee 2, the LASL experiment on Imp 8, the Massachusetts Institute of Technology experiment on Imp 8, and the Goddard Space Flight Center (GSFC) electron spectrometer of Isee 1.

The boxed graphs in Figure 2 show the distributions of solar wind fluid parameters and IMF directions obtained by *Formisano et al.* [1974]. We would expect distributions representing the 1977 epoch of our data to be comparable to those of Formisano et al., so we presume that in our case the Alfvén Mach number M_A, the proton thermal to field energy ratio β_p, and the polar angle of the IMF, indicated by the arrows in the respective distributions, were all close to the long-term modes (i.e., most probable values) of these quantities in the solar wind. The one exception was the ecliptic angle of the IMF, which at 105° was more perpendicular to the sun-earth line

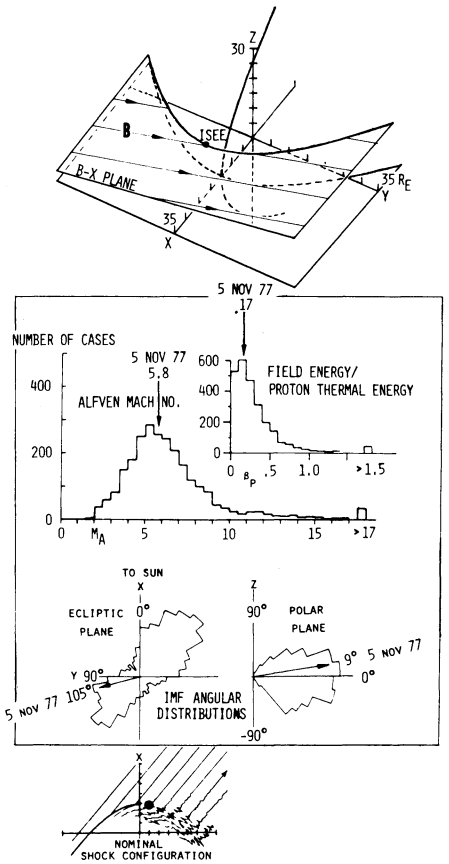

Fig. 2. Geometric and plasma parametric context of the November 5, 1977, inbound bow shock crossings by Isee 1 and 2.

(the X axis) than usual. The only result of this deviation from the long-term average was to make the bow shock perpendicular at the location of the Isee crossings when the most probable, or nominal IMF, at 135°, would ordinarily have made the shock locally quasi-parallel, as in the bottom sketch.

The last quantity, T_e/T_p, in Table 1 is known to have been appreciably outside its normal range in the solar wind. The mode, median, and mean of the T_e/T_p distribution tabulated by *Feldman et al.* [1977] from Imp 6 data were 1.2, 1.6, and 2.0, respectively, with 90% of their values falling between 0.6 and 4.6. However, T_e/T_p was about 12 before the crossings of November 5, 1977, described here. This was an extraordinarily high ratio, and one often expected to trigger current-driven ion acoustic instabilities [*Gurnett et al.*, 1979]. Thus we deal with the parameter set of 'typical' quasi-perpendicular bow shock, not far from the subsolar point, where corrections for nonnormal preshock flow can be considered negligible, but under conditions unusually favorable to current-driven instability. Allowing for the T_e/T_p level applicable to this shock observation, we have here a bow shock typical of the cold, dense, slow solar wind preceding a high-speed stream [*Gurnett et al.*, 1979].

TABLE 1. Solar Wind Parameters

Parameter	Value
V, km/s	300
N, cm^{-3}	8
T_e, °K	2.4×10^5
T_p, °K	2×10^4
arccos (**B** · **n**), deg	68
M_a, M_{MS}	5.7, 3.3
β_p, β	0.17, 2.2
T_e/T_p	12

THE SHOCK SIGNATURE

Fluid Profile

The major measurements characterizing the fluid parameters of the solar wind are shown in Figure 3 for Isee 1's crossing of the bow shock. Although differing in small details, the crossing at Isee 2 was essentially the same for all the depicted quantities. The remarkable similarity of shock profiles at one spacecraft to those at the other has been illustrated for several cases in an earlier publication [*Russell and Greenstadt*, 1979], so we avoid repetition here. The nature of the small differences can be appreciated by examining the two magnetic profiles in Figure 1 and the discussion by Russell and Greenstadt.

In the uppermost three panels of Figure 3 the proton parameters appear only after the time of shock crossing because the channel spacing of the instrument and the coldness of the solar wind combined to produce incomplete ion distributions and inconsistent moments. The principal observations we extract from Figure 3 are as follows (from top to bottom, but with continual reference to the magnetic shock 'front' defined by the bottom plot (vertical dotted line)):

1. The magnetic field displayed a small gradual rise, or 'foot,' corresponding to the increases in electron density, temperature, and northward flux, outside the front. Behind the front the field formed a squarelike overshoot, containing a train of oscillations that correspond to the overshoots in electron temperature and density.

2. The solar wind density was incremented by about 54% of its ultimate total jump by the time the front was crossed.

3. The solar wind proton 'temperature' completed much of its total jump earlier than or just after the time the front

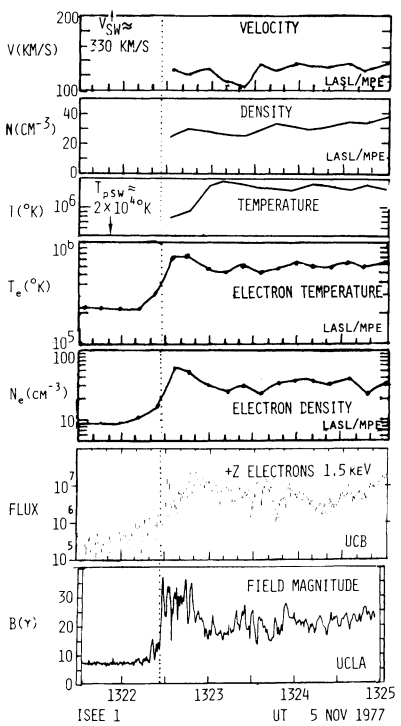

Fig. 3. Plasma fluid parameters through the shock crossing at Isee 1.

was crossed and ultimately rose to more than 2.5 times the downstream electron temperature.

4. The electron temperature and density both reached peak, or 'overshoot,' values just behind the front before relaxing to their magnetosheath values further downstream. These peaks were also described by *Bame et al.* [1979].

5. The electron heating, as indicated by the high–time resolution flux measurements of the portion of the 1.5-keV electron distribution that was deflected northward (second panel from bottom), occurred on average as a smooth rise starting ahead of the front and continuing through it to about where the peaks in electron density and temperature ended.

In addition, we have examined the individual ion energy distributions closely (Figure 4) and find from the peaks that the solar wind was appreciably reduced in velocity from its upstream value and was approaching its downstream value by the time it crossed the front.

Ion and Plasma Wave Profile

In and around the shock transition proper the plasma was not in equilibrium, and the fluid parameters useful for indicating general conditions in the solar wind could not give an accurate description of shock dynamics. At the boundary it was therefore necessary to examine particle and wave spectra and to monitor particles with the highest resolution available. The most basic measurements are shown in Figure 4.

The four main panels of Figure 4 display (from top to bottom) (1) four representative channels of the plasma wave analyzer over the full range of sampled frequencies, (2) the flux of northward (±7.5°) directed protons of about 1.5 keV, (3) the magnetic field magnitude, and (4) the plasma wave spectral response from 0 to 1 kHz. In between, and superimposed on the second and third panels, is a string of inserts representing the solar wind ion energy spectra centered in the ecliptic (±55°) and sampled every 12 s (every fourth spectrum). In terms of the real horizontal time scale the energy sweep of each spectrum begins at the high-energy end of its voltage channels, at the real time corresponding to the left (low energy) edge of the box, and ends 3 s later, before the beginning of the next box. The energies are plotted in the conventional way from low to high, with the 0.1- and 1-keV points as indicated in the first box. Electron spectra are omitted from Figure 4 because their relatively smooth and regular behavior was adequately represented by the density and temperature graphs of Figure 3.

The most important features of Figure 4 are the persistent nonthermal shapes of the ion distributions and their relationship to the field profile. The two bimodal distributions of 1322:09 and 1322:21 in particular are striking. They correspond to the foot and the sudden jump in the field designated the 'front' in the preceding section and figure. They were preceded by skewed, irregular distributions containing high-energy particles supplemental to the solar wind, and they were followed by heated, variable, bimodal distributions in which the two peaks eventually merged to form a single, skewed, repeatable distribution about 1 min past the end of the figure.

The second bimodal distribution associated with the front, recorded at 1322:21, was clearly distinct from the first post-

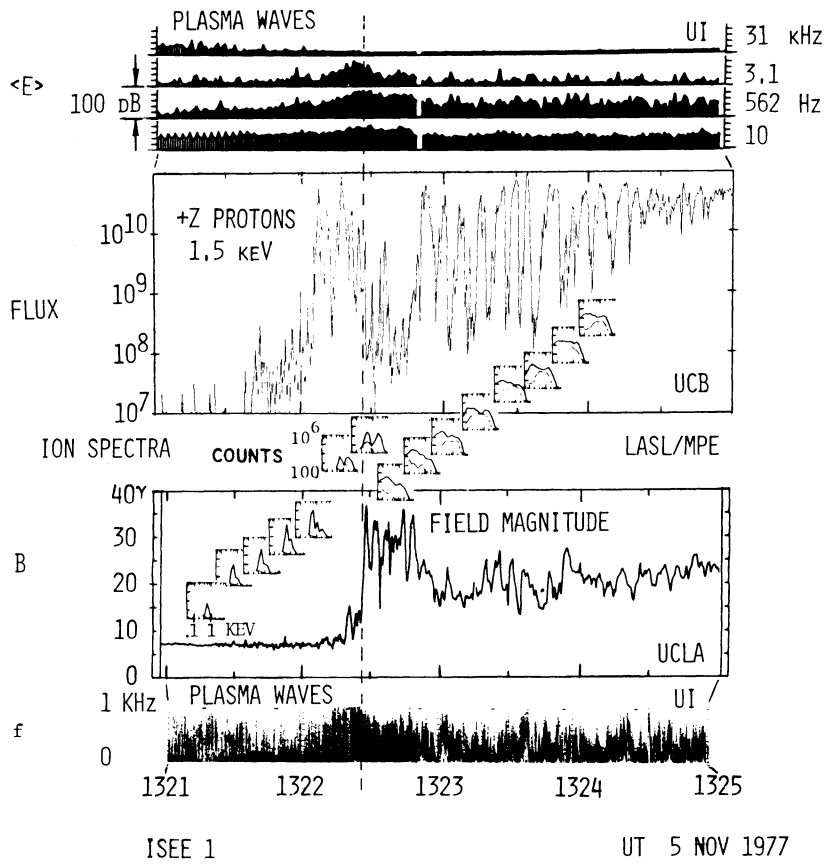

Fig. 4. Selected details of field and particle data through the shock crossing at Isee 1. The heavy and light lines in the small spectral inserts represent data from solar and antisolar hemispheres, respectively.

shock distribution, since the right-hand ends of the two spectra were different. Thus the high-energy end of the spectrum that began at 1322:21 was not simply a partial trace of the heated distribution that immediately followed. It may be inferred then that a significant and very sudden contribution to the heating of the ions was made almost exactly at 1322:33, just behind the 'front,' and about one quarter of the way through the square-shaped overshoot wave train of the magnetic field.

No obvious single event corresponding to the apparent ion heating layer was recorded by the plasma wave detector. The bottom panel in Figure 4 shows that the most intense electric wave noise in the ion acoustic (and lower hybrid) frequency range below 1 kHz occurred between 1322:20 and 1322:50, accompanying the bimodal ion distributions and the magnetic foot and overshoot, but no single striking enhancement appeared at the available resolution in this panel at 1322:33.

The northward ion flux panel above the magnetic field plot shows several arresting features. Most prominent, in the context of the other measurements, is the preshock flux enhancement between 1322:10 and 1322:30. This burst of particles evidently represented a separate view of the second peak of the bimodal solar wind distributions, indicating that the velocities of the particles contributing to the second peak were widely distributed in latitude. Since the IMF was close to the ecliptic (Figure 2), the northward flux enhancement implies the presence of ions of high pitch angle. The identification of the $+Z$ ions with the second peak stems from the location of the peak at 2 keV, not far from the 1.5-keV window of the Berkeley instrument.

The prominence of the preshock burst arises in part from its next most distinguishing feature, namely, its attenuation at the actual shock front and throughout the 20-s magnetic field overshoot. Since the second peak of the postfront solar wind spectra was close to 1.5 keV and since there was little change in direction of **B** across the front, we infer that the interval of attenuated flux occurred because there were fewer particles in the northward direction.

Following the field overshoot, the persistence of bimodality, the variations in shape from one distribution to the next, and the varying differences between solar and antisolar spectral curves indicated incomplete thermalization of the ions. The postshock incompleteness of proton thermalization was confirmed by the $+Z$ flux that, following its attenuation, rose on average through a series of oscillations to a settled value where the spectra also steadied down just beyond the end of the figure, as was mentioned earlier. The behavior of the particles at Isee 2 was essentially parallel to, but displaced in time from, that described here.

Taken together, the particles and field data suggest that a group of accelerated particles, with its peak at $E/E_{SW} \approx 3.3$ or $V/V_{SW} \approx 1.8$, existed in the solar wind outside the shock front. These particles should not be thought of only as locally reflected protons, but also ions passing by in the direction of $-(\mathbf{B} + \mathbf{V}_{SW} \times \mathbf{B})$ after reflection elsewhere along the shock. From this group a subset, slightly decelerated along with the solar wind, penetrated the front and was heated together with the main solar wind distribution, forming a bimodal postshock spectrum that ultimately became a single, skewed distribution several minutes downstream.

The plasma wave strips at the top of Figure 4 exhibit samples of the local electric field behavior throughout the frequency range of the instrument. We see that electron plasma oscillations at 31 kHz persisted in the solar wind up to the foot of the shock, declining just where the rise in electron density (Figure 3) moved the oscillations above the frequency of the 31-kHz band. Waves of 3.1 and 0.56 kHz probably representing the Doppler-shifted ion acoustic mode [*Rodriguez and Gurnett,* 1975], rose in amplitude as the shock was approached and reached maximal intensity just at or outside the front. There is a hint in the figure that 3- and 0.4-kHz noise reached local maxima just before 1322, near the first detection of the group of reflected ions. This particular observation, which was more pronounced in many wave channels at Isee 2, suggests an additional 'boundary' phenomenon at the forward edge of the 'foot.' The 0.56-kHz noise persisted in the magnetosheath well above its solar wind level and was marked by numerous bursts of enhanced amplitude. The 10-Hz noise seems to have increased in the foot of the shock, maximized just behind the front, and continued high through the field overshoot. It may be here, around the lower hybrid resonance, that the appropriate correlation with the abrupt ion heating at 1322:33 is to be found. However, a 10-Hz noise maximum behind the front was not evident at Isee 2.

We note finally that Figure 4 shows, from 1321:25 to 1322:10, the first association between very small field oscillations outside a quasi-perpendicular shock and the presence of suprathermal shock-related ions in the solar wind distributions, visible in the small inserts.

DISCUSSION

Major Features

The data presented in the foregoing figures offer both verification of earlier results and identification of new details of the earth's shock structure neither measured nor predicted before.

Two important attributes of shock structure are clearly confirmed by these early data. First, the qualitative order of events in the shock transition was substantially the same as that constructed earlier from diverse observational sources. A selection of items from Figures 3 and 4 of this report could be juxtaposed that would almost reproduce the schematic shock profile created from separate papers to illustrate an earlier review [*Greenstadt,* 1976]. These items would be the magnetic field profile (ignoring short-period oscillations), the proton spectra, the shape of the electron to proton temperature ratio, the plasma wave spectrogram, and the electron plasma oscillation band (31-kHz band). Furthermore, the field profile and double proton spectra have the essential qualitative relationship to each other sketched from theoretical sources by *Tidman and Krall* [1971, Figure 7.9]. Second, the initial proton heating appears to have occurred suddenly within a small slice of the shock transition, as was observed earlier by *Ossakow et al.* [1970] and discussed in relation to theoretical predictions of double shocks at high Mach number by *Tidman and Krall* [1971, Figure 7.7].

The significance of these observations of major features of the shock should not be underrated with the misunderstanding that they are routine confirmations of former results. They are not composites of scattered measurements and do not involve inferences of relevant parameters but rather represent comprehensive measurements of interrelated variables in a given case under known conditions. Nevertheless, it is worth noting how representative the double ion distributions of *Montgomery et al.* [1970] and *Formisano and Hedgecock* [1973] were to those documented more formally here. The full

value of this set of measurements will be reached, of course, when compared later with other cases in which marginal or threshold levels of the various parameters can be seen to control the appearance and disappearance of individual features.

The new shock elements evident here consist of the details of the reflected ion distribution, revealed by the UCB device, including the directional angle discrimination before and behind the shock 'front,' the oscillatory ion thermalization interval, with its very regular periodicity, revealed by the high time resolution of the UCB instrument, and the double foot with its small and large magnetic oscillations attended by absence or presence of northward protons and divided by a boundary effect sufficiently strong to excite local plasma waves. The very high upstream T_e/T_p may have been responsible for the boundary effect, which may not occur in other cases. These characteristics of the shock need to be fitted into theoretical models of the high β, high M boundary, but in so doing, the caution expressed by *Tidman and Krall* [1971, p. 131] is strongly endorsed by the data of this report: The plasma actually impinging on the shock front at high M is two ion gases different from the traditional upstream fluid and must be so defined. Moreover, the moment-derived experimental parameters in and immediately surrounding the front cannot be taken at face value because the peculiar ion distributions do not lend themselves to routine processing and must eventually be represented in another way. Certainly, it appears that individual, or bunched, particle orbits will need to be taken into account in a full shock model.

Shock Potential

Quantitative evaluations of theoretical models, scale lengths, and energy balances will be described in a separate report. It is instructive, however, to include here one very rough calculation of shock potential as a first-order guide to what can be achieved with the Isee instrumentation, even for low-resolution observations.

Most theoretical attacks on collisionless shock dynamics, at least those that lead to definable, measurable quantities, deal with simplified conditions, e.g., subcritical M, perpendicular **B**, cold ions, etc. The November 5 case was none of these but was close enough to justify a simple exercise that exposes its discrepancies to study. We use a very simple set of formulas developed by *Morse* [1973] for a perpendicular, laminar (subcritical), resistive shock. Since our shock was not quite perpendicular ($\theta_{nB} \approx 70°$), was slightly supercritical ($M_{MS} \gtrsim 3$), and involved substantial ion heating, we should expect a definite discrepancy between theory and observation. We show this by estimating the velocity drop from the shock potential.

The formulas we use are (mks)

$$\Delta\phi = \frac{B_1(B_2 - B_1)}{e\mu_0 N_1} + \frac{5}{2}(T_{e2} - T_{e1}) \qquad (1)$$

and

$$\Delta\phi = \frac{m_i}{2e}(V_1^2 - V_2^2) \qquad (2)$$

where $\Delta\phi$ is the integrated potential across the shock, subscripts e, 1, and 2 refer to electrons, upstream values, and downstream values, and m_i is the ion mass. These equations, which are expressions (10) and (14) of *Morse* [1973], have the advantage that no reference to (often ambiguous) shock thickness is required. The formula can be employed any place where measurements of B, T_e, and V are available.

We see in Figure 3 that the flow velocity did not stabilize until about 1323:30, so we need to pick more than one set of downstream values to represent the shock process. We use the four times and field levels marked on the magnetic profiles of Figure 1 for both Isee 1 and Isee 2. The first time (t_1) is upstream, and the remainder (t_2, t_3, t_4) are at various points 'downstream,' where a subscript 2 is indicated in the equations above. For example, $\Delta\phi_3 = B_1(B_3 - B_1)/e\mu_0 N_1 + 5(T_{e3} - T_{e1})/2$, where appropriate temperatures (and velocities) can be read from Figure 3. The points selected correspond to the first available V, at the top of the foot (t_2), the overshoot readings (t_3), and the early stabilized flow (t_4). The field values taken were visual averages, and the temperatures were interpolated levels between measurements. Isee 1 and 2 values were alike except at time t_2.

The first four columns after the time identification in Table 2 outline the computation according to (1) and (2), with

$$V = (V_1^2 - 2e\Delta\phi/m_i)^{1/2}$$

We see immediately from Figure 3 that V according to calculation was considerably greater at every point than the corresponding measured value. The sixth column of Table 2 lists the discrepancy δV between calculated and measured quantities, i.e., $\delta V_i = V_i - V_{\text{meas}}(t_i)$. Thus the solar wind was slowed down, even at the earliest time t_2, much more than could be accounted for by electron heating alone.

The obvious place to look for the missing bulk velocity is in the proton temperature. The last column of the table gives the proton temperature equivalents δT_p of the δV's. But the maximal difference between upstream and downstream proton temperatures measured or, more accurately, constructed by the data processing scheme, anywhere, was about 20×10^5 °K. It appears then that the imputed observed proton heating did not account for all of the missing bulk velocity either, especially in the shock front.

Candidate phenomena to take up the lost energy are wave propagation, dispersion and radiation, particle reflection, and separate streaming of the second ion distribution. We do not pursue the matter further in this report but merely note that the discrepancy is consistent with what should be expected from application of an idealized model to a nonideal case and with the observation in that case of several features excluded from the model's assumptions. Identification of the role played by each phenomenon is the objective of further study.

TABLE 2. Perpendicular Shock Potential Relations for Electron Heating Alone

Time t_i	ΔB, γ	ΔT_e, 10^4 °K	$\Delta\phi_i$, eV	V_i, km/s	δV_i, km/s	δT_p, 10^5 °K
t_2, Isee 1	5.5	16	58.3	312	152	43
t_2, Isee 2	10	26	99.4	299	139	39
t_3	22	80	268	239	109	24
t_4	14	60	190	269	129	32

Maximum measurement, ≈20.

CONCLUSION

A completely 'typical' shock crossing is not so easy to find, even with the best instrumentation. To the extent that the November 5, 1977, crossings represented such a case, however, at least in front of a high-speed stream, the shock profile offered several unanticipated structural features. These were a variable directional profile of the reflected proton group passing through the front, an electrostatic boundary effect associated with the reflected protons upstream, and an oscillatory buildup of proton thermalization behind the 'overshoot' portion of the shock signature. An idealized shock potential calculation, together with the details of ion energy distributions in and around the front, indicates that the reduction of supersonic to subsonic flow affected by the shock was accomplished by diverting a fraction of the flow energy to processes other than electron and proton heating.

Acknowledgments. The help of K. Ogilvie, J. Scudder, and R. Elphic is very much appreciated. This work has been supported by National Aeronautics and Space Administration contracts and grants NASW-3007 (TRW), NAS5-20064 (UCLA), NAS5-20079 (UCB and University of Washington), NAS5-2093 (University of Iowa), and S-50864A (LASL). Los Alamos' participation was under the auspices of the U.S. Department of Energy, Max-Planck-Institut's, under that of the German Bundesministerium für Forschung und Technologie (RV14-B6/74).

The Editor thanks D. H. Fairfield and another referee for their assistance in evaluating this paper.

REFERENCES

Anderson, K. A., R. P. Lin, R. J. Paoli, G. K. Parks, C. S. Lin, H. Rème, J. M. Bosqued, F. Martel, F. Cotin, and A. Cros, An experiment to study energetic particle fluxes in and beyond the earth's outer magnetosphere, *IEEE Trans. Geosci. Electron., GE-16,* 213, 1978.

Bame, S. J., J. R. Asbridge, H. E. Felthauser, J. P. Glore, G. Paschmann, P. Hemmerich, K. Lehmann, and H. Rosenbauer, Isee 1 and Isee 2 fast plasma experiment and the Isee 1 solar wind experiment, *IEEE Trans. Geosci. Electron., GE-16,* 216, 1978.

Bame, S. J., J. R. Asbridge, J. T. Gosling, M. Halbig, G. Paschmann, N. Sckopke, and H. Rosenbauer, High temporal resolution observations of electron heating at the bow shock, *Space Sci. Rev., 23,* 75, 1979.

Feldman, W. C., J. R. Asbridge, S. J. Bame, and J. T. Gosling, Plasma and magnetic fields from the sun, in *The Solar Output and Its Variations,* edited by O. R. White, J. A. Eddy, and D. Heath, p. 351, University of Colorado Press, Boulder, 1977.

Formisano, V., The physics of earth's collisionless shock wave, *J. Phys. Paris, 38,* C6–65, 1977.

Formisano, V., and P. C. Hedgecock, On the structure of the turbulent bow shock, *J. Geophys. Res., 78,* 6522, 1973.

Formisano, V., G. Moreno, and E. Amata, Relationships among the interplanetary plasma parameters: Heos 1, December 1968 to December 1969, *J. Geophys. Res., 79,* 5109, 1974.

Gosling, J. T., J. R. Asbridge, S. J. Bame, G. Paschmann, and N. Sckopke, Observations of two distinct populations of bow shock ions in the upstream solar wind, *Geophys. Res. Lett., 5,* 957, 1978.

Greenstadt, E. W., Phenomenology of the earth's bow shock system: A summary description, in *Magnetospheric Particles and Fields,* edited by B. M. McCormac, p. 13, D. Reidel, Hingham, Mass., 1976.

Greenstadt, E. W., and R. W. Fredricks, Shock systems in collisionless space plasmas, in *Solar System Plasma Physics: A Twentieth Anniversary Review,* vol. 3, edited by C. F. Kennel, L. J. Lanzerotti, and E. N. Parker, p. 4, North-Holland, Amsterdam, 1979.

Gurnett, D. A., F. L. Scarf, R. W. Fredricks, and E. J. Smith, The Isee 1 and Isee 2 plasma wave investigation, *IEEE Trans. Geosci. Electron., GE-16,* 225, 1978.

Gurnett, D. A., E. Marsch, W. Pilipp, R. Schwenn, and H. Rosenbauer, Ion acoustic waves and related plasma observations in the solar wind, *J. Geophys. Res., 84,* 2029, 1979.

Knott, K., A. Durney, and K. Ogilvie (Eds.), *Advances in Magnetospheric Physics With Geos 1 and Isee,* D. Reidel, Hingham, Mass., 1979.

Montgomery, M. D., J. R. Asbridge, and S. J. Bame, Vela 4 plasma observations near the earth's bow shock, *J. Geophys. Res., 75,* 1217, 1970.

Morse, D. L., Electrostatic potential rise across perpendicular shocks, *Plasma Phys., 15,* 1262, 1973.

Ossakow, S. L., G. W. Sharp, and K. K. Harris, Spectrometer observations in the region near the bow shock on March 12, 1968, *J. Geophys. Res., 75,* 6024, 1970.

Parks, G. K., C. Gurgiolo, S. Lin, K. A. Anderson, R. P. Lin, F. Martel, and H. Rème, Dual spacecraft observations of energetic particles in the vicinity of the magnetopause, bow shock, and the interplanetary medium, *Space Sci. Rev., 22,* 765, 1978.

Paschmann, G., N. Sckopke, G. Haerendel, and J. Papamastorakis, Isee plasma observations near the subsolar magnetopause, *Space Sci. Rev., 22,* 717, 1978.

Rodriguez, P., and D. A. Gurnett, Electrostatic and electromagnetic turbulence associated with the earth's bow shock, *J. Geophys. Res., 80,* 19, 1975.

Russell, C. T., The Isee 1 and 2 fluxgate magnetometers, *IEEE Trans. Geosci. Electron., GE-16,* 239, 1978.

Russell, C. T., and E. W. Greenstadt, Initial Isee magnetometer results: Shock observations, *Space Sci. Rev., 23,* 3, 1979.

Tidman, D. A., and N. A. Krall, *Shock Waves in Collisionless Plasmas,* Interscience, New York, 1971.

(Received August 6, 1979;
revised December 19, 1979;
accepted January 10, 1980.)